Published in final edited form as:
Electrophoresis. 2011 November ; 32(22): 3172–3179. doi:10.1002/elps.201100229.

Characterization of Cell Lysis Events on a Microfluidic Device for High-Throughput Single Cell Analysis

Amy D Hargis, **JP Alarie**, and **J.M. Ramsey***
Department of Chemistry, Chapman Hall Room 251, University of North Carolina at Chapel Hill, Chapel Hill, North Carolina 27599-3216

Abstract

A microfluidic device capable of rapidly analyzing cells in a high-throughput fashion using electrical cell lysis is further characterized. In the experiments performed, cell lysis events were studied using an EMCCD camera with high frame rate (> 100 fps) data collection. It was found that, with this microfluidic design, the path that a cell follows through the electric field affects the amount of lysate injected into the analysis channel. Elimination of variable flow paths through the electric field was achieved by coating the analysis channel with a polyamine compound to reverse the electroosmotic flow (EOF). EOF reversal forced the cells to take the same path through the electric field. The improved control of the cell trajectory will reduce device-imposed bias on the analysis and maximizes the amount of lysate injected into the analysis channel for each cell, resulting in improved analyte detection capabilities.

Keywords

Single Cell; Microfluidics; Cell Lysis

1 INTRODUCTION

Traditional cell signaling studies are performed as ensemble averages of cellular response. In ensemble averaging, the lysate of a large number of cells is pooled to obtain sufficient analyte for detection and to rapidly screen the cells' collective responses. This type of analysis obscures individual cell behavior and can provide misleading results [1]. To acquire accurate information on cellular signaling, cells should be analyzed individually, in a manner in which data on a large number of individual cells can be collected.

One obstacle in studying cellular processes at the single cell level is that genetically identical cells are heterogeneous in their chemical composition, response to external stimuli and biological activity [2–6]. This heterogeneity requires analysis of a large number of cells so that statistically significant and relevant conclusions can be made regarding cellular activity. Furthermore, many analytes are present in low copy numbers, which makes detection difficult [7–9]. Because cellular signaling is known to change on a very short timescale, each cell should be analyzed in as short a time as possible [6,10–11]. Short analysis times are also needed to minimize the total experiment time. To date, technology to

Correspondence: J. M. Ramsey, Chapman Hall Room 251, Chapel Hill, NC 27719, jmramsey@email.unc.edu, Phone: 919-962-7492, Fax: 919-962-2388.

CONFLICT OF INTEREST STATEMENT
The authors declare that there are no conflicts of interest in publishing this work.

perform this type of high-throughput, single cell analysis of intracellular processes has not been well established.

In the past, single cell chemical analysis has been performed using capillary electrophoresis (CE) methods [6–8,12–15]. These techniques are elegant in their ability to separate and detect a large number of analytes from a single cell but suffer from low throughput [6,8,11,15–18]. Typical CE methods are capable of analyzing only 10 to 35 cells per day due to the labor intensive methods required to prepare and inject cells into a capillary [11,19–20]. High-throughput single cell analysis has been achieved using flow cytometry, yet the technique is limited in the number of intracellular analytes that can be detected from a single cell due to the need for fluorescent tags with different spectral characteristics for each analyte [17]. Thus, electrophoretic analysis is desired for the simultaneous interrogation of multiple analytes from a single cell. Recently, microfluidic technology has demonstrated great promise for increasing the throughput of electrophoretic single cell analysis [6,10–11,21]. Through proper microchip design, cells can be easily manipulated throughout the device and the cell's microenvironment carefully controlled to reduce the stress that a cell experiences [10]. Additionally, very high electric fields can be generated within the short channels of a microchip allowing for fast analyte separation [11]. Finally, the precise fluid handling capabilities of a microchip limits the post-lysis sample dilution and lower limits of detection can be achieved.

To date, a few reported devices have demonstrated the lysis of individual cells and subsequent analyte detection from the cell lysates [22–23]. These early stage devices display faster throughput rates compared to traditional CE methods. For instance, Gao and workers report 15 cells per hour throughput on their device [23] and Munce and collaborators report an analysis rate of approximately 24 cells per hour [22]. Although these devices demonstrate rapid cell analysis compared to CE methods, they are still somewhat labor intensive in their transport of cells to a lysis region. Therefore, their ultimate utility may be limited by the time required to collect large data sets.

In this paper, we discuss improvements to a previously reported microfluidic device that is capable of analyzing intracellular analytes in a high throughput fashion [21]. The device, shown in Figure 1, is capable of analyzing single cells at rates up to 7–12 cells per minute. The device operates by hydrodynamically flowing cells through an electric field where subsequent electrical cell lysis occurs. The resulting cell lysate is electrokinetically injected into the analysis channel for electrophoretic separation and laser induced fluorescence (LIF) detection. A focusing channel just prior to the cell lysis intersection constricts the cell flow path and forces the cells into approximate single file for LIF detection. The single file flow of cells through the laser creates a cytometric signal that marks the on-set of the lysate separation. Since its initial introduction, development has focused on characterizing the device and making it amenable to collection of large data sets of biologically relevant information. The work described here aims to improve the flow of cells through the device to eliminate device-imposed bias from cell to cell. As a result, an increase in individual cell analyte detection capabilities and quantification accuracy will be made possible.

During device characterization, it was observed that the cell flow path across the lysis intersection is one of the factors that can affect the amount of lysate that injects into the analysis channel. Analyte loss can be problematic for detection of low level analytes; thus, improving lysate injection efficiency will remove device-imposed bias and allow for improved lysate injection. We demonstrate that, by controlling the surface charge on the analysis channel, we can eliminate variability in the cell flow path across the lysis intersection. This improved control ensures that each cell experiences a similar environment

throughout the analysis and will reduce potential device-imposed bias on the individual cell analyses.

2 MATERIALS AND METHODS

Chemicals

Unless otherwise stated, all chemicals were purchased from Sigma (St. Louis, MO, USA). B270 glass substrates, with chrome and positive photoresist (AZ1518) pre-applied, were purchased from Telic Company (Valencia, CA, USA).

Microchip Fabrication

The microfluidic channel network layout is shown in Figure 1. All microchips were fabricated from 50 mm × 50 mm, 0.9 mm thick B270 crown glass using traditional photolithography techniques and wet chemical etching methods described elsewhere [24–26]. Channel access holes were milled through the substrate at the ends of the channels using aluminum oxide powder blasting (Microblaster, Comco Inc., Burbank, CA). The etched substrate was fusion bonded to a 0.9 mm thick B270 cover slip to create a closed channel network [24]. Buffer and sample reservoirs were created by attaching cloning cylinders (Fisher Scientific, 4 mm i.d.) around the access holes using Norland 63 Optical Adhesive (Norland Products, Inc., Cranbury, NJ). Each reservoir holds a volume of approximately 100 μL. To connect a syringe pump to the chip, a 1/16″ barbed female Luer lock (Upchurch Scientific, Oak Harbor, WA) was altered by removing the barb and drilling an ~ 3 mm hole into the bottom using a Dremel tool. This Luer lock was then epoxied onto the top of the cell waste reservoir. 1/16″ i.d. tubing was attached to the female Luer lock via a 1/16″ barbed male Luer lock (Upchurch Scientific).

Several different microchips were used for this study. Channel depths and widths were determined using a stylus-based surface profiler (P-15; KLA-Tencor, Mountain View, CA). Widths are reported as the full channel width measured at the top of the channel. All channels were etched to a depth between 20 – 25 μm. The cell flow (CF) flow channel and the cell waste (CW) channel were 65–80 μm wide. The analysis (A) channel from the lysis intersection to the 90° turn and the narrow section of the separation buffer (SB) channel were 45–60 μm wide. The wide sections of all the channels were 255–270 μm wide. The analysis channel from the lysis intersection to the 90° turn was 20.0 mm long and the distance between the tee intersection of the focusing (F) channel with the cell flow channel and the lysis intersection was approximately 105 μm.

Pluronic Channel Coating

To reduce cell adhesion to the glass surfaces, the channels were coated with a 30% (w/w) solution of Pluronic F-127 (BASF, Mount Olive, NJ) in water. The channels were prepared by first rinsing with 1 N NaOH for approximately 1 hour. The channels were then flushed with water followed by a 1 hour rinse with the Pluronic F-127 solution. Because the Pluronic F-127 solution is highly viscous at room temperature, the microchip was kept on an ice block during the Pluronic coating procedure to ensure that the solution and channels remain at approximately 4°C. The channels were subsequently flushed with water, to remove excess Pluronic, and air-dried by emptying the reservoirs and pulling vacuum on the waste channel.

Electroosmotic Flow Reversal

The chip was prepared with the Pluronic F-127 as stated above, however, only the cell flow channel was coated. This was accomplished by placing the 30% (w/w) Pluronic F-127 solution into the cell flow and focusing reservoirs only. Water was placed in the separation

buffer and analysis reservoirs and vacuum pulled on the cell waste reservoir to coat. After coating, the channels were rinsed with water to remove excess Pluronic solution. Immediately following the Pluronic coating procedure, the analysis channel was dynamically coated with a polyamine compound, PolyE323 (synthesis and structure described elsewhere) [27–28]. This coating was performed by placing a 6% (v/v) solution, pH 7.0, of PolyE323 in the separation buffer and analysis reservoirs. Water was placed in all other reservoirs. Vacuum was then applied to the cell waste channel for approximately 1 hour to pull the PolyE323 compound through the analysis channel to cell waste. The channels were then rinsed with water. All channels, except for the focusing channel, were filled with separation buffer for the experiments. The focusing channel was filled with a 50:50 mixture of separation buffer and 1% (v/v) Triton-X surfactant. The Triton-X was used to aid in removing cellular debris that often collects within the lysis intersection during chip operation.

Cell Culture and Preparation

Jurkat Cells (ATCC TIB-152, American Type Culture Collection, Rockville, MD; obtained from the University of North Carolina Tissue Culture Facility) were used for all experiments. The cell cultures were maintained at 37°C and 5% CO_2 in RPMI 1640 1× Medium (Gibco BRL, Gaithersburg, MD) supplemented with 10% (v/v) fetal bovine serum, 100 μg/mL Penicillin and 100 μg/mL Streptomycin. The cells were grown in 25-mL polystyrene culture flasks (Nalge Nunc International, Rochester, NY) to densities of approximately 1×10^6/mL before passage.

To load the cells with dye, ~1×10^6 cells were pelleted (1000g for 3 minutes) and the supernatant discarded. The cells were then re-suspended in a solution of 50 μM Oregon Green 488 carboxylic acid diacetate 6-isomer and extracellular buffer (ECB: 135 mM NaCl, 15 mM KCl, 2 mM $MgCl_2$, 2 mM $CaCl_2$, 10 mM HEPES, pH 7.4). Oregon Green in diacetate form is membrane permeable and cell loading was achieved through simple incubation (~20 minutes) in a centrifuge vial while maintaining the cells at 37°C. The cells were then washed 3 to 4 times by pelleting and re-suspended in ECB containing 10 mM Glucose.

Device Operation and Data Collection

The electrophoresis buffer consisted of 50 mM TRIS, 10 mM Boric Acid, 1 mM Spermine, 1 mM TCEP-HCl and 30 mM PEG (MW 200 g/mol), pH 9.0. The loaded cells were transferred to the cell flow reservoir and the separation buffer, analysis and waste channels were filled with the separation buffer. The focusing channel was filled with a 1:1 mixture of the separation buffer and 1% (v/v) Triton-X surfactant. The chip was positioned on a microscope (Nikon Eclipse TE2000-U, 10X objective) to observe the cell flow and lysis events. Cell fluorescence was observed by excitation with a mercury lamp. The emission light was filtered through a Semrock (Rochester, NY) Brightline GFP-3035B-NTE filter.

To operate the chip, cells were hydrodynamically pulled across the cell flow channel by applying negative pressure to the cell waste reservoir using a syringe. The negative pressure was applied manually and was adjusted until the flow of cells from the cell flow reservoir was approximately 0.5 mm/s. The pressure on the waste channel outlet was monitored using a pressure transducer circuit (data not shown) and demonstrated <5% pressure variation throughout the duration of the data collection period. Platinum electrodes, placed in the separation buffer and analysis reservoirs were used to apply a DC voltage for both electrical cell lysis and electrophoretic lysate separation. The electric field was applied only along the separation buffer and analysis channels. The voltage was supplied by a Bertan power supply (Model 2866A, Bertan, Hicksville, NY). For all reported experiments, +8 kV was applied to

the analysis channel electrode relative to the separation buffer reservoir. This applied voltage gave electric field values between 2400 to 2600 V/cm along the analysis channel between the 90° turn and the channel intersection where lysis occurs. The hydrodynamic flow was adjusted with the attached syringe until cell lysis was observed.

Cell lysis images were obtained using a Cascade II EMCCD camera (Photometrics, Tucson, AZ) controlled by the NIS-Elements Advanced Research software package (Nikon, Melville, NY). The camera was set to collect at the maximum frame rate possible and was operated at −80°C. Both the NIS-Elements Basic and Advanced Research software packages were used to analyze the collected videos and to determine the xy-coordinates for plotting the cell flow paths through the microfluidic device. A cell's xy-coordinates were measured at the approximate center of the observed cell. For cells traveling with a 0.5 mm/s average flow velocity, the cell trajectories were plotted by determining the xy-coordinates of a cell approximately every 5 frames of the lysis video as the cell traveled between the sample reservoir to the area just prior to the focusing channel. Once the cell reached the focusing channel, the cell's xy-coordinates were determined for each frame of the video. For cells traveling at 2.0 mm/s, the xy-coordinates of the cell were determined for each frame of the video. The xy-positions of the cell were then plotted in Microsoft Excel to provide a visual image of the cell flow path.

For cell simulations, 10-μm diameter fluorescently labeled polystyrene beads (Polysciences, Inc., Warrington, PA) diluted in ECB were used. The bead solutions were placed in the cell flow reservoir and pulled through the chip in the same manner as the cells. The same electric fields used for the cell experiments were applied for the bead experiments, where applicable. For electroosmotic flow analysis, a concentrated solution of Rhodamine B, a neutral marker [29], was placed in the cell flow reservoir and pulled through the chip in the same manner as the cells and beads.

3 RESULTS AND DISCUSSION

Rapid cell lysis is critical to accurately capture the state of intracellular analytes [11,19]. When the microchip operation was previously described [21], complete cell lysis was reported to occur in fewer than 33 milliseconds (ms). Due to camera frame rate limitations (max 30 frames per second (fps)), an accurate cell lysis time measurement was difficult to determine because, in images taken of lysis events, the cells appear intact in one frame and completely lysed in the subsequent frame. It was apparent from those collected images that electrical cell lysis occurs faster than 33 ms. In this study, higher frame rate data acquisition of on-chip cell lysis events have been collected using a Cascade II EMCCD camera. The region of interest used to capture the cell lysis event images is shown in Figure 2a. Typical frame rates for this set-up ranged from approximately 100 to 160 fps and the cell lysis events were observed at intervals of ~6–10 ms, allowing for more precise determination of cell lysis event timing.

A sequence of frames from a cell lysis event recorded at 133 fps (8 ms/frame) is shown in Figure 2b. At high electric fields, irreversible damage to the cell membrane occurs. It can be inferred that once lysate is observed to be leaving the cell, the cell is lysed. In the image shown in Figure 2b, the cell enters the lysis intersection in frame 1 and lysate is observed to begin exiting the cell in frame 2. Thus, the cell was lysed within approximately 8 ms. Another lysis event is shown in Figure 2c. In this instance, the cell enters the lysis intersection in frame 2 and lysate is observed to be exiting the cell in frame 4. This cell required approximately 16 ms to lyse. Collection of videos at a higher frame rate has provided the ability to observe more details about the on-chip electrical lysis of the cells and has allowed for more accurately defined lysis rates.

In studying the electrical lysis rates, we noticed inconsistency in the lysate injection that occurred from cell to cell. In some instances, the lysate of a cell appeared to completely inject into the analysis channel as it passed through the lysis intersection, shown in Figure 2b. In these cases, as the cell lysed (frames 1 and 2, respectively), it remained in the lysis intersection long enough for the lysate to eject from the membrane and inject into the analysis channel (frames 3–5). The cell membrane debris then continued with the hydrodynamic flow (frames 6–8) down the cell waste channel. In other instances, the lysate did not fully inject into the analysis channel before the cell membrane continued to waste. An example of this is shown in the images of Figure 2c. This type of event appeared to result in significant loss of cell lysate to waste. Attempts to quantify the amount of lysate injected versus that lost to waste were difficult due to the presence of the fluorescent cell membrane post-lysis, as can be observed in Figure 2. The post-lysis cell membrane often traveled amongst the lysate that was lost to waste and affected the quantification of the amount of fluorescence due only to lysate. Therefore, qualitative assessments were made as to the extent of lysate injected by observing the flow of lysate at the lysis intersection.

Our goal here was to determine the cause of the observed differences in lysate injection events and, if possible, try to control the flow of cells through the device to reduce the possibility of analyte loss. Because biofouling often occurred at the lysis intersection during chip operation, only a limited number of cells could be analyzed in a single run of the device. In one run, a total of 72 cells were recorded and it was observed that four different event types took place within the lysis intersection, two of which involved cell lysis and two showed a complete lack of cell membrane rupture. The two lysis events were labeled as ”type A”, to describe instances where the majority of a cell’s lysate appeared to inject into the analysis channel and the membrane flowed to cell waste, and “type B”, to describe events where the cell lysate was partially injected into the analysis channel and a significant portion was lost down the cell waste channel. The non-lysis events were termed “whole cell injected”, to describe events in which the cell was injected intact into the analysis channel, and “no lysis”, to denote an event in which the cell passed through the lysis intersection into the cell waste channel without lysing. Of the 72 cells recorded, 43 cells were observed to undergo lysis type A and 24 cells were of lysis type B. Only one cell was whole cell injected and four cells fell into the no lysis category. In this particular study, we were concerned with understanding the variability of cell lysate injection into the analysis channel. Therefore, the study focused only on the cells that lysed within the channel intersection.

Using the video still frame images, the cell flow paths through the microchip lysis intersection were plotted by determining the cell’s x- and y-coordinates. Representative cell flow paths were plotted for lysis type A and B events and are shown in Figure 3. Figure 3a displays the flow path of the cells of lysis type A. All cells in this lysis category take a similar flow path in which their trajectory involves a small deviation into the analysis channel during the lysing process. On the other hand, the flow paths for lysis type B all deviate within the lysis intersection toward the separation buffer channel, as seen in Figure 3b. It is believed that, because these cells take a path away from the analysis channel entrance, the electrokinetic injection force is not strong enough to overcome the hydrodynamic force; therefore, a significant portion of the lysate is transported to the cell waste channel.

It is known that the linear velocity of a cell through the lysis intersection will have an affect on the lysis event. The flow rate affects the exposure time of a cell to the electric field, which determines the extent of lysis and, in turn, will affect how much lysate injects into the analysis channel. However, we observed that even for cells that are traveling at approximately the same linear velocity, several of the event types were observed at the lysis intersection. Examples of the lysis events and the corresponding cell linear velocities for a

series of cells lysed in a single run of the device are shown in Table 1. As can be seen from these examples, although the linear velocities are similar, three of the event types were observed. The three type A cells shown were all traveling at approximately 0.50 mm/s. The type B cell was actually traveling at a slightly slower linear velocity than the type A cells. The cells that were whole cell injected had linear velocities both above and below that of the type A cells. Of the lysis events studied overall, a correlation between linear velocity and lysis type (i.e., A vs B) was not observed.

With cell velocity eliminated as a possible cause, additional theories to explain the differing flow paths focused on cell membrane heterogeneity and electroosmotic effects at the lysis intersection. It is well-established that genetically identical cells vary in terms of their size, intracellular chemical composition and exterior membrane composition. This heterogeneity could affect their behavior within the electric field used for lysis [2–6]. To eliminate the effect of cell heterogeneity, 10-μm diameter fluorescent polystyrene beads were used to simulate the cells. The beads are similar in size to Jurkat cells yet have uniform surface charge [10]. The previous experiments were repeated with a solution of beads placed in the sample reservoir. The resulting flow paths, with and without an electric field applied (Figure 3c–d) were plotted. With no electric field applied, the beads followed the expected path through the lysis intersection as flow from the focusing channel pushed them towards the entrance of the analysis channel. Upon application of an electric field, all of the beads followed an upward flow path similar to that of the type B cells. This cathodic flow of the negatively charged beads indicated that a residual EOF may be present within the separation buffer and analysis channels.

The presence of a residual EOF in the Pluronic coated channels was investigated using Rhodamine B, a neutral fluorescent marker. A solution of Rhodamine B was pulled through the chip in the same manner as the cells. A fluorescence image of the Rhodamine B flow path is shown in Figure 4a. With the electric field applied, a small percentage of Rhodamine B was observed to flow up the separation buffer channel, confirming the presence of a cathodic EOF. The majority of the flow, however, showed the same upward deflection seen with the type B cells and continues on to the cell waste reservoir. In fact, when the flow paths for the type B cells were overlaid with the Rhodamine B flow path (data not shown), the upward deflections seen for both flows align. This indicated that the residual EOF was the cause for the upward flow path of the type B cells.

To achieve maximum lysate injection for each cell as it passes through the lysis intersection, the flow path analysis indicated that their path should deviate toward the analysis channel during lysis (Figure 3a). Currently, a consistent flow path is not achieved with the Pluronic coating, which leads to the various lysate injection events. A possible way to ensure that cells take the type A flow path would be to increase the flow toward the anode. This was tested by creating an anodic EOF within the separation buffer and analysis channels. The EOF reversal within these channels was achieved by coating with a polyamine compound, PolyE323 [27–28]. This compound interacts electrostatically with the glass surface and results in a large number of amine groups exposed to the bulk solution. The cell flow and waste channels were still coated with Pluronic F-127 to retain their cell anti-adhesive properties. Figure 4b demonstrates the EOF reversal with Rhodamine B now flowing towards the anode upon application of the electric field. The experiment using 10-μm diameter fluorescently labeled beads was repeated and showed that, with the EOF reversed, the bead flow paths are now consistent with the type A cell flow paths (Figure 5a).

With the EOF reversed, the lysis event variability was tested. Cells were loaded with Oregon Green diacetate cytosolic dye to visualize the lysis events. The chip was prepared as described above with Pluronic F-127 on the cell flow and waste channels and PolyE323 on

the separation buffer and analysis channels. The flow paths were then observed and plotted with several of the cell paths shown in Figure 5b. In one run of the device, 25 cell paths were recorded before significant cellular debris buildup was observed in the lysis intersection. All cells were observed to take the optimal trajectory for efficient lysate injection. Due to the combination of a cell's electrophoretic mobility towards the anode coupled with the strong anodic EOF, a greater hydrodynamic velocity (2 mm/s) was required to prevent whole cell injection. The higher cell velocity reduced the extent of deviation into the analysis channel compared to the original experiments and reduced the cell exposure time to the electric field. The results of these experiments were that all lysed cells fell into the type A flow path category, but only 56% of the cells lysed (i.e., there were more "no lysis" events). We consider the gain in consistent injection efficiency worth the loss in lysis efficiency.

It is noted for future experiments that the hydrodynamic force pulling the cells through the electric field needs to be carefully controlled. This is to ensure that the appropriate cell linear velocity is achieved for maximum lysate injection. Here, the change in the analysis channel coating procedure to reverse the EOF allows for greater control over the cell flow path through the lysis intersection. This device improvement forces each cell to experience similar flow paths through the lysis intersection and will reduce potential bias in the individual cell analyses.

4 CONCLUDING REMARKS

An EMCCD camera with high frame rate video acquisition provided the ability to observe on-chip cell lysis events and injection of the cell lysate into the analysis channel for characterization of a microfluidic device for single cell analysis. From this information, it was noted that the cell flow paths through the lysis intersection have an effect on the amount of lysate that injects into the analysis channel. The current channel coating used to reduce biofouling did not provide complete electroosmotic flow suppression, which resulted in flow path variability. By reversing the electroosmotic flow within the analysis channel, a consistent flow path of cells through the device was achieved, which was consistent with events in which cell lysate fully injects into the analysis channel.

Future work for this device includes more precise control of the cell velocity through the channel network and additional channel coating studies to reduce biofouling at the lysis intersection, which will result in the ability to collect larger data sets.

Acknowledgments

We thank Dr. Nancy Allbritton and Dr. Kevin Braun for helpful discussions and technical assistance. This research was supported by a grant from the NIH (5-RO1-GM0607905-03). ADH was also supported by a fellowship from Merck & Co.

List of Abbreviations

EMCCD	Electron Multiplying Charge Coupled Device
CF	Cell Flow
CW	Cell Waste
A	Analysis
SB	Separation Buffer
F	Focusing

ECB	Extracellular buffer
DC	Direct Current

References

1. Ferrell JE, Machleder EM. Science. 1998; 280:895. [PubMed: 9572732]
2. Sweedler JV, Arriaga EA. Analytical and Bioanalytical Chemistry. 2007; 387:1.
3. Breslauer DN, Lee PJ, Lee LP. Molecular Biosystems. 2006; 2:97. [PubMed: 16880927]
4. Sims CE, Bachman M, Li GP, Allbritton NL. Analytical and Bioanalytical Chemistry. 2007; 387:5. [PubMed: 16955263]
5. Danna EA, Nolan GP. Current Opinion in Chemical Biology. 2006; 10:20. [PubMed: 16406766]
6. Huang WH, Ai F, Wang ZL, Cheng JK. Journal of Chromatography B-Analytical Technologies in the Biomedical and Life Sciences. 2008; 866:104.
7. Zhang ZR, Krylov S, Arriaga EA, Polakowski R, Dovichi NJ. Analytical Chemistry. 2000; 72:318. [PubMed: 10658325]
8. Woods LA, Roddy TP, Ewing AG. Electrophoresis. 2004; 25:1181. [PubMed: 15174037]
9. Hellmich W, Pelargus C, Leffhalm K, Ros A, Anselmetti D. Electrophoresis. 2005; 26:3689. [PubMed: 16152668]
10. Price AK, Culbertson CT. Analytical Chemistry. 2007; 79:2614. [PubMed: 17476726]
11. Sims CE, Allbritton NL. Lab on a Chip. 2007; 7:423. [PubMed: 17389958]
12. Kennedy RT, Oates MD, Cooper BR, Nickerson B, Jorgenson JW. Science. 1989; 246:57. [PubMed: 2675314]
13. Zabzdyr JL, Lillard SJ. Trac-Trends in Analytical Chemistry. 2001; 20:467.
14. Jankowski JA, Tracht S, Sweedler JV. Trac-Trends in Analytical Chemistry. 1995; 14:170.
15. Woods LA, Ewing AG. Analytical and Bioanalytical Chemistry. 2003; 376:281. [PubMed: 12774183]
16. Stuart JN, Sweedler JV. Analytical and Bioanalytical Chemistry. 2003; 375:28. [PubMed: 12520431]
17. Chen SJ, Lillard SJ. Analytical Chemistry. 2001; 73:111. [PubMed: 11195493]
18. Gao N, Wang WL, Zhang XL, Jin WR, Yin XF, Fang ZL. Analytical Chemistry. 2006; 78:3213. [PubMed: 16643017]
19. Sims CE, Meredith GD, Krasieva TB, Berns MW, Tromberg BJ, Allbritton NL. Analytical Chemistry. 1998; 70:4570. [PubMed: 9823716]
20. Borland LM, Kottegoda S, Phillips KS, Allbritton NL. Annual Review of Analytical Chemistry. 2008; 1:191.
21. McClain MA, Culbertson CT, Jacobson SC, Allbritton NL, Sims CE, Ramsey JM. Analytical Chemistry. 2003; 75:5646. [PubMed: 14588001]
22. Munce NR, Li JZ, Herman PR, Lilge L. Analytical Chemistry. 2004; 76:4983. [PubMed: 15373432]
23. Gao J, Yin XF, Fang ZL. Lab on a Chip. 2004; 4:47. [PubMed: 15007440]
24. Madou, MJ. Fundamentals of microfabrication : the science of miniaturization. 2nd ed.. Boca Raton: CRC Press; 2002.
25. Jacobson SC, Koutny LB, Hergenroder R, Moore AW, Ramsey JM. Analytical Chemistry. 1994; 66:3472.
26. Jacobson SC, Hergenroder R, Koutny LB, Warmack RJ, Ramsey JM. Analytical Chemistry. 1994; 66:1107.
27. Hardenborg E, Zuberovic A, Ullsten S, Soderberg L, Heldin E, Markides KE. Journal of Chromatography A. 2003; 1003:217. [PubMed: 12899312]
28. Ullsten S, Zuberovic A, Wetterhall M, Hardenborg E, Markides KE, Bergquist J. Electrophoresis. 2004; 25:2090. [PubMed: 15237410]

29. Wang W, Zhou F, Zhao L, Zhang JR, Zhu JJ. Journal of Chromatography A. 2007; 1170:1. [PubMed: 17915240]

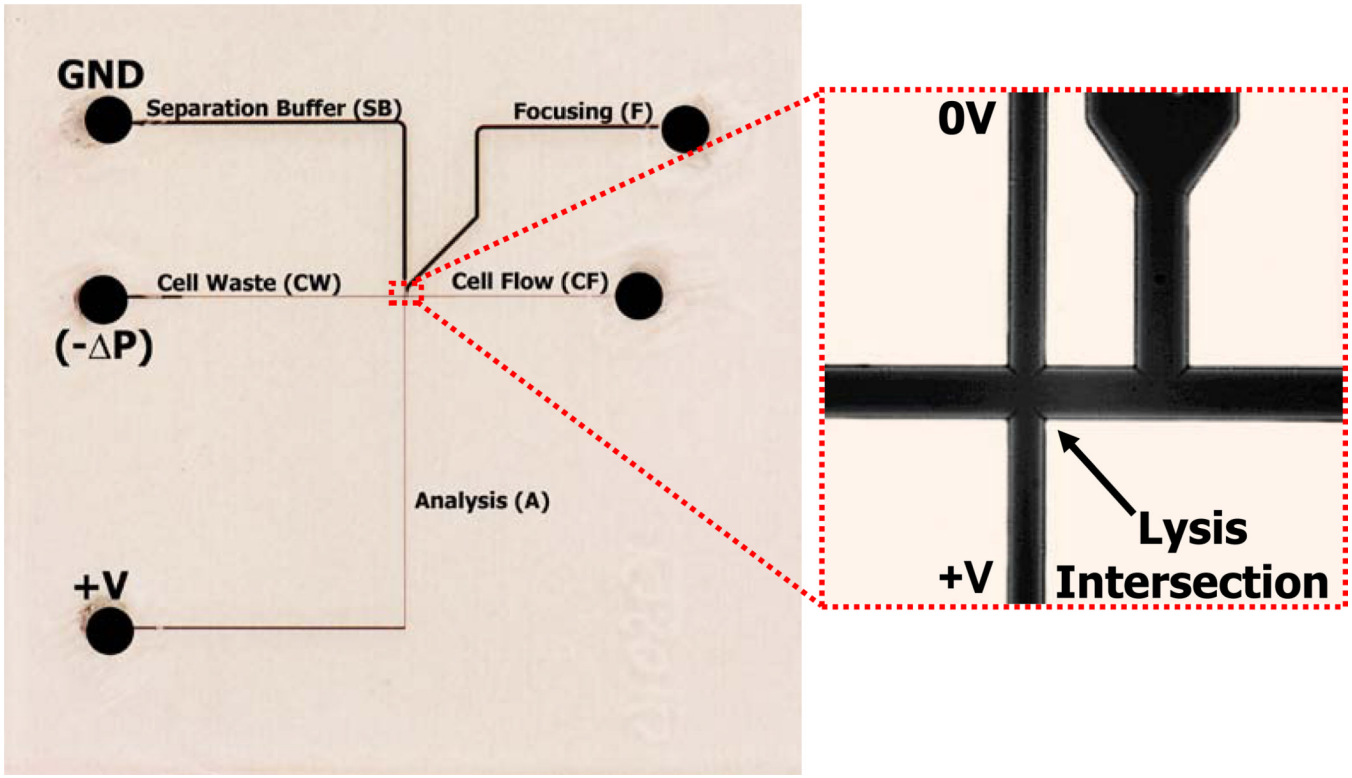

Figure 1.
Image of microfluidic channel network with close up image of the channel network and lysis intersection. Channels are filled with black ink for visualization; Cells are focused to single file, prior to entering the lysis intersection, by the focusing channel (F). At the lysis intersection cells encounter the applied DC electric field and dielectric breakdown of the cell membrane occurs. The cell lysate is electrokinetically injected into the analysis channel (A) and the cell membrane and uncharged debris flow to cell waste (CW) with the hydrodynamic flow. All channels were etched to a depth between 20 – 25 μm. Channel widths are reported as the full width measured at the top of the channel and are as follows; cell flow (CF) channel and CW were 65–80 μm, A from the lysis intersection to the 90° turn and the narrow section of the separation buffer (SB) channel were 45–60 μm, wide sections of all the channels were 255–270 μm. The analysis channel from the lysis intersection to the 90° turn was 20.0 mm long and the distance between the tee intersection of the focusing (F) channel with the cell flow channel and the lysis intersection was approximately 105 μm.

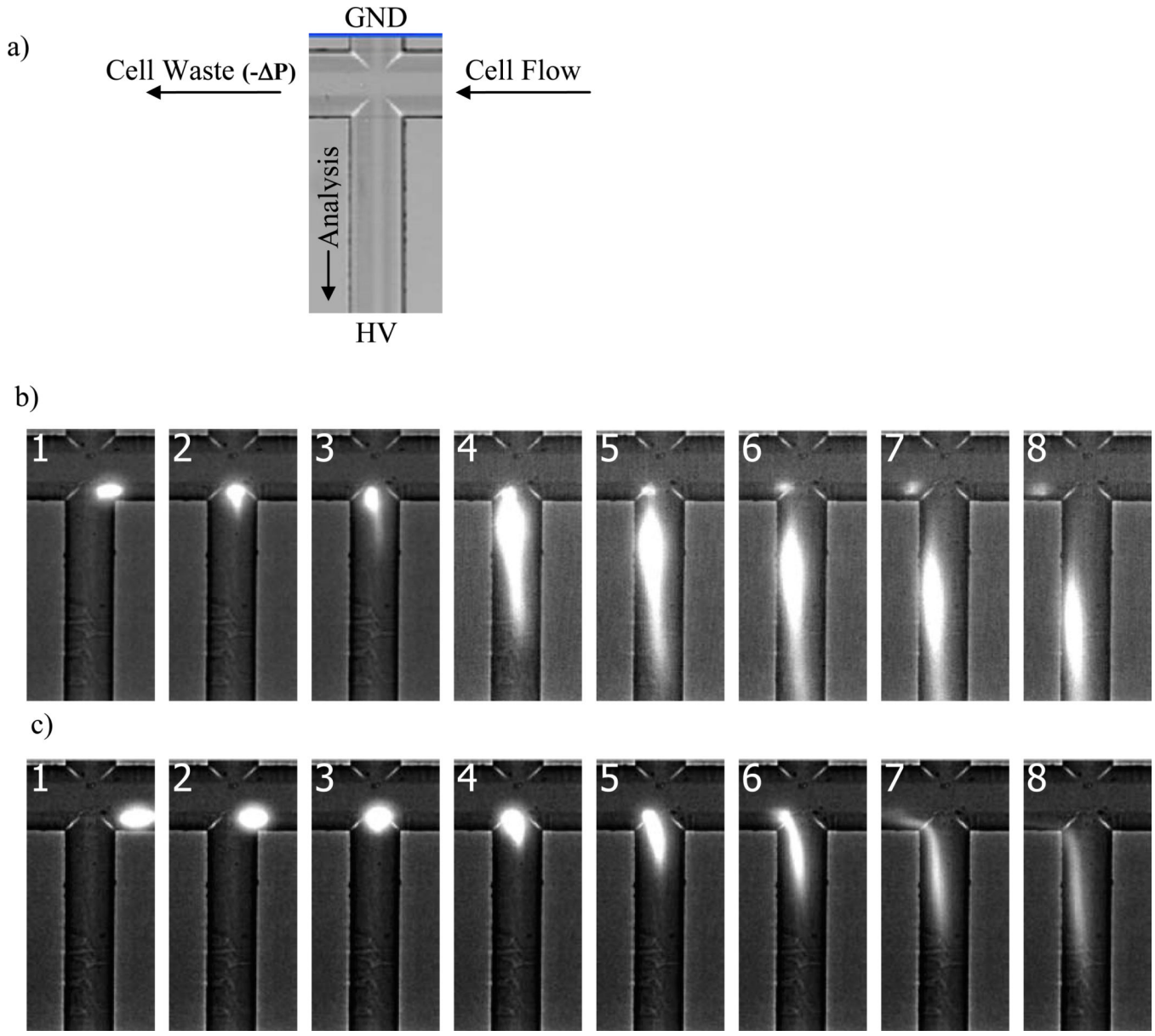

Figure 2.

Sequential images of cell lysis events collected at 132 fps (8 ms/frame). a) White light image of chip showing the region of interest (ROI) captured; b) Images of a cell lysis event in which the majority of the lysate is injected into the analysis channel. Images 1–2 display the cell lysing. Images 3–6 display the cell lysate ejecting from the cell membrane within the channel intersection. Images 7–8 show the flow of the cell membrane to waste and the migration of the cell lysate (Oregon Green) down the analysis channel to the detection point; c) Images of a cell lysis event in which a significant portion of the cell lysate is lost to waste. Images 6–8 demonstrate the flow of some cell lysate down the cell waste channel with the cell membrane post-lysis.

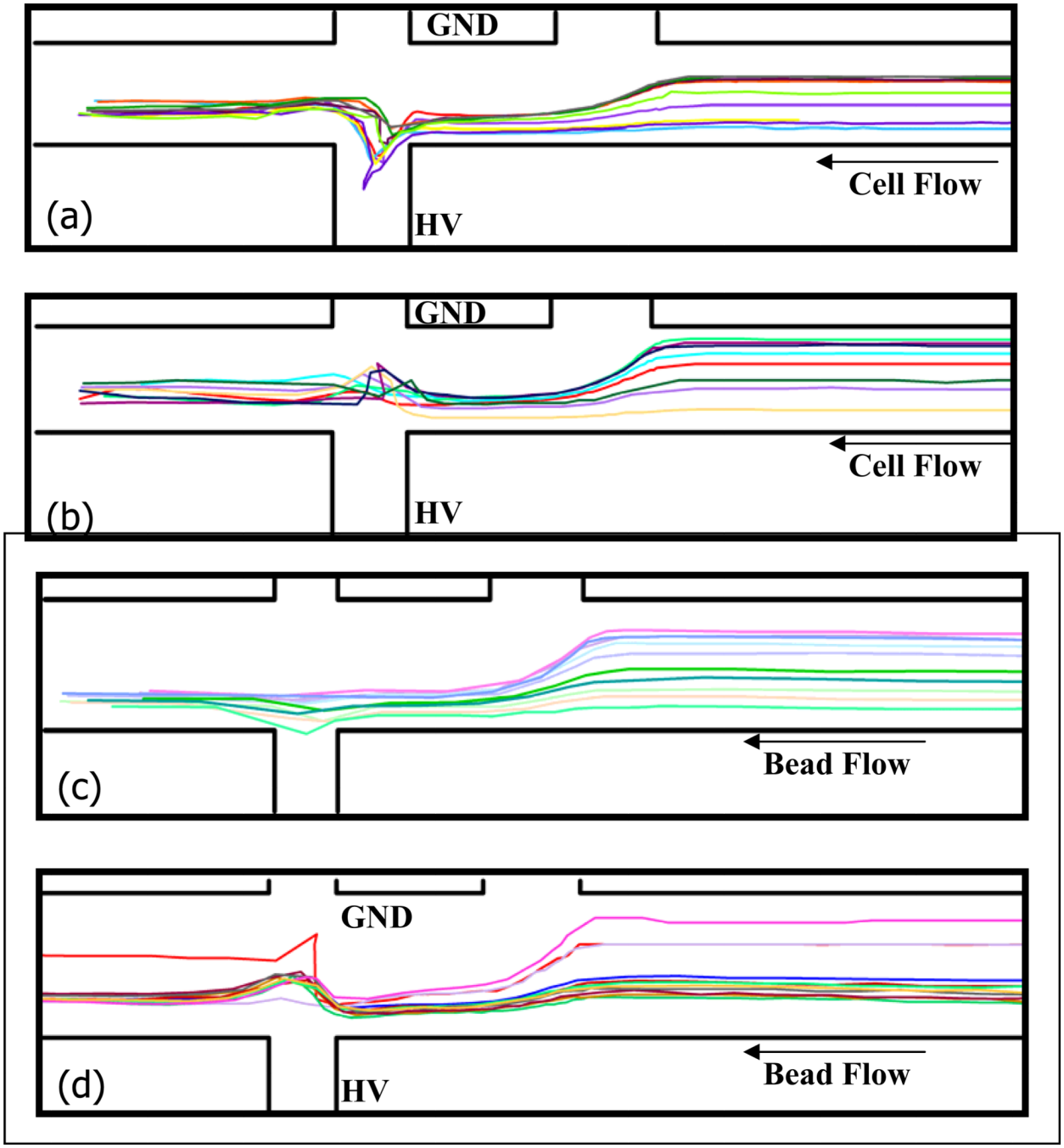

Figure 3.
Cell flow paths plotted for a) lysis events in which the majority of lysate is injected into the separation channel (Type A events) and b) lysis events in which a significant amount of cell lysate is not injected and flows with the hydrodynamic flow to waste (Type B events). Plotted flow paths of 10-μm diameter fluorescently labeled polystyrene beads with c) no electric field applied along the analysis channel and d) electric field applied along the analysis channel

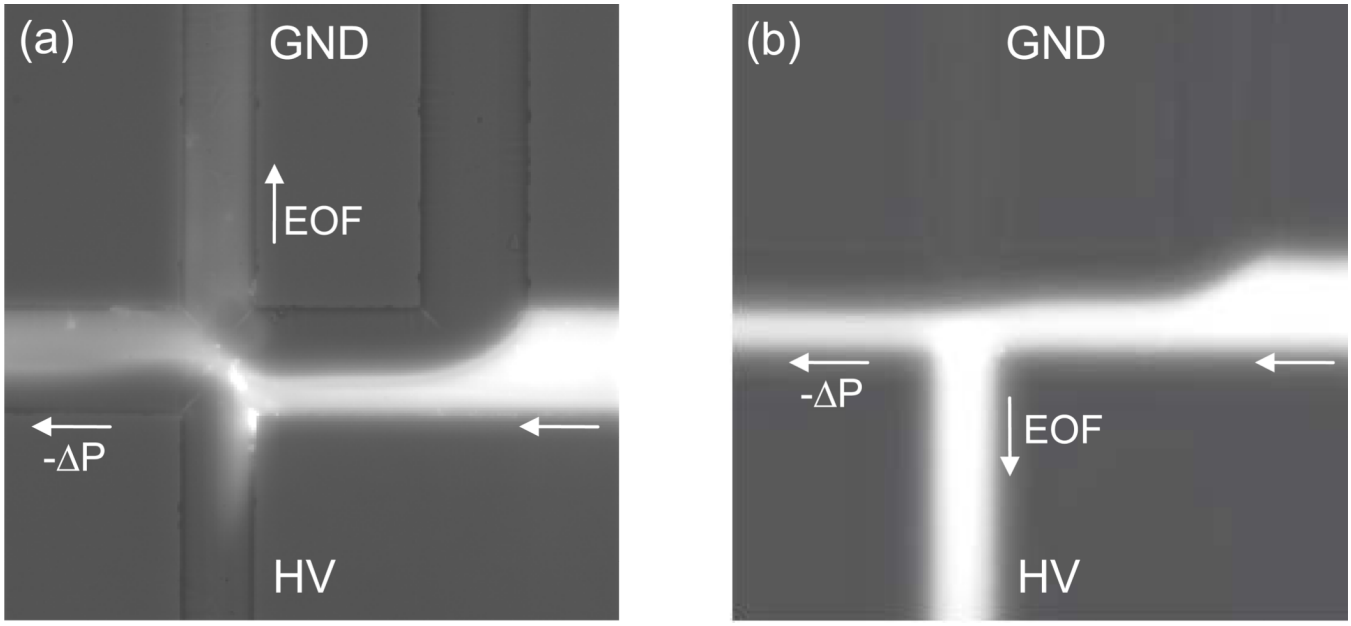

Figure 4.

Images displaying the Rhodamine B flow path to visualize the direction of electroosmotic flow within the analysis channel. Rhodamine B is pulled from the sample reservoir to waste through application of negative pressure on the waste reservoir. A DC electric field is applied along the analysis channel. In a) the analysis channel is coated with Pluronic F-127 and the EOF is observed to be slightly cathodic. In b) the EOF is reversed by coating the analysis channel with a polyamine compound, PolyE323. The flow of Rhodamine B to the anode confirms the EOF reversal.

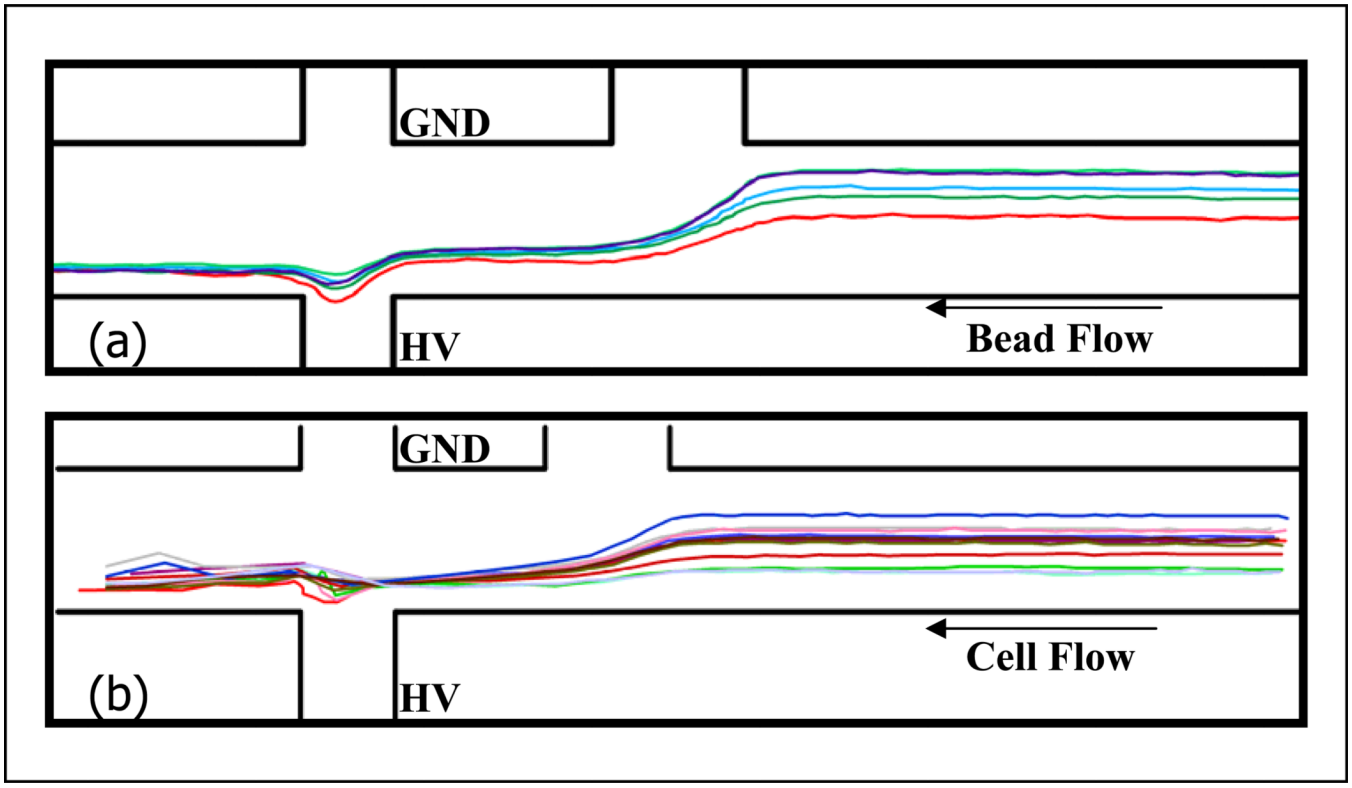

Figure 5.

Plotted flow paths of a) beads and b) cells after electroosmotic flow reversal within the analysis channel. In a) 10-μm diameter fluorescently-labeled polystyrene beads all demonstrate a flow path in which they deviate into the analysis channel due to the pull of the anodic EOF. This flow path is similar to that of the type A cells. The flow path of Jurkat cells through the lysis intersection with the EOF reversed can be seen in b). All cells were observed to take similar flow paths.

Table 1

Event types and corresponding linear flow rates for cells that passed through the lysis intersection.

Cell Number	Event Type Observed	Cell Linear Flow Rate (mm/s)
1	Type A	0.50
2	Whole Cell Injection	0.51
3	Type B	0.32
4	Type A	0.49
5	Type A	0.50
6	Whole Cell Injection	0.42